

Experimental investigation of a general real-time 3D target localization method using sequential kV imaging combined with respiratory monitoring

Byungchul Cho^{1,2}, Per Poulsen^{1,3,4}, Dan Ruan¹, Amit Sawant¹
and Paul J Keall^{1,5}

¹ Department of Radiation Oncology, Stanford University, Stanford, CA, USA

² Department of Radiation Oncology, Asan Medical Center, University of Ulsan College of Medicine, Seoul, Korea

³ Department of Oncology, Aarhus University Hospital, Aarhus, Denmark

⁴ Institute of Clinical Medicine, Aarhus University, Aarhus, Denmark

⁵ Radiation Physics Laboratory, Sydney Medical School, University of Sydney, Sydney, Australia

E-mail: paul.keall@sydney.edu.au

Received 4 April 2012, in final form 16 August 2012

Published 24 October 2012

Online at stacks.iop.org/PMB/57/7395

Abstract

The goal of this work was to experimentally quantify the geometric accuracy of a novel real-time 3D target localization method using sequential kV imaging combined with respiratory monitoring for clinically realistic arc and static field treatment delivery and target motion conditions. A general method for real-time target localization using kV imaging and respiratory monitoring was developed. Each dimension of internal target motion $\mathbf{T}(x, y, z; t)$ was estimated from the external respiratory signal $R(t)$ through the correlation between $R(t_i)$ and the projected marker positions $\mathbf{p}(x_p, y_p; t_i)$ on kV images by a state-augmented linear model: $\mathbf{T}(x, y, z; t) = \mathbf{a}R(t) + \mathbf{b}R(t - \tau) + \mathbf{c}$. The model parameters, \mathbf{a} , \mathbf{b} , \mathbf{c} , were determined by minimizing the squared fitting error $\sum \|\mathbf{p}(x_p, y_p; t_i) - \mathbf{P}(\theta_i) \cdot (\mathbf{a}R(t_i) + \mathbf{b}R(t_i - \tau) + \mathbf{c})\|^2$ with the projection operator $\mathbf{P}(\theta_i)$. The model parameters were first initialized based on acquired kV arc images prior to MV beam delivery. This method was implemented on a trilogy linear accelerator consisting of an OBI x-ray imager (operating at 1 Hz) and real-time position monitoring (RPM) system (30 Hz). Arc and static field plans were delivered to a moving phantom programmed with measured lung tumour motion from ten patients. During delivery, the localization method determined the target position and the beam was adjusted in real time via dynamic multileaf collimator (DMLC) adaptation. The beam-target alignment error was quantified by segmenting the beam aperture and a phantom-embedded fiducial marker on MV images and analysing their relative position. With the localization method, the root-mean-squared errors of the ten lung tumour traces ranged from 0.7–1.3 mm and 0.8–1.4 mm during the single arc and five-field static beam delivery, respectively. Without the localization method, these errors ranged from 3.1–7.3 mm. In summary, a general method

for real-time target localization using kV imaging and respiratory monitoring has been experimentally investigated for arc and static field delivery. The average beam-target error was 1 mm.

(Some figures may appear in colour only in the online journal)

Introduction

Three dimensional knowledge of tumour location during abdominal and thoracic radiotherapy is an important component of motion management whether the treatment delivery utilizes motion inclusive, gating or tumour tracking methods. A wide variety of real-time or continuous localization methods are either available or under development. The diversity of systems includes radiofrequency, radioisotope, ultrasound and MRI, in addition to the optical, kV and MV imaging systems available on conventional accelerators. In this study, we experimentally investigated a method for real-time localization and delivery adaptation, that uses a commercially-available, gantry-mounted kV imaging system combined with optical respiratory monitoring.

The rationale for utilizing a method combining kV imaging with optical respiratory monitoring was its widespread clinical availability: kV imaging is available from most major linear accelerator vendors including Accuray, BrainLab, Elekta and Varian. kV imaging enables image-based target localization and geometry monitoring independently of the megavoltage treatment beam, at a cost of imaging dose. Stereoscopic kV imaging has been explored for intrafraction radiotherapy guidance (Shirato *et al* 2000b, 2000a, Berbeco *et al* 2004, Hoogeman *et al* 2009, Kamino *et al* 2006), yet most commercial systems do not offer stereoscopic kV imaging. A 3D localization method using a single gantry-mounted kV imager has been experimentally studied by Poulsen *et al* (2010a; 2010c), yielding geometric uncertainties of approximately 1.5 mm for arc and static delivery to abdominal, thoracic and prostate targets. In order to reduce the imaging dose, it is appealing to combine kV imaging with an external respiratory signal and develop an internal/external correlation model (Murphy *et al* 2007). Respiratory monitors are widely available in medicine and relatively cheap devices, such as a web-cam (Siwiak *et al* 2009) and the iPod accelerometer (Lam *et al* 2009) have been used to provide a useful respiratory signal.

Pioneering work combining internal and external signals using *stereoscopic* x-ray imaging and a respiratory signal for target localization was performed by Schweikard *et al* (2000) and incorporated into the Cyberknife linear accelerator. Several further models have been proposed (Murphy 2004, Isaksson *et al* 2005, Kanoulas *et al* 2007) and one has been integrated into a prototype dynamic multileaf collimator (DMLC) tracking system and experimentally investigated (Cho *et al* 2011). However, not all IGRT systems have imagers capable of synchronous stereoscopic imaging. Furthermore, even for those systems capable of stereoscopic imaging, it may not be optimal to image synchronously to balance targeting accuracy and imaging dose. The challenge with using a single imager for target localization is that the position along the imaging beam is difficult to determine. In an earlier work, Cho *et al* (2008) described a method of combining a single kV imager with a respiratory signal, where the position along the imaging beam was estimated by building a correlation model between the unresolved component and the two other components projected on the imager from prior information of the 3D target trajectory. This method was evaluated for fixed beam simulation studies. More recently, a new sequential model has been developed in which the

internal/external correlated model is updated by a minimization of the difference between the measured projections and the estimated trajectory projected into the imaging geometry (Cho *et al* 2010). The method is general enough to be applicable to a wide variety of IGRT systems and to be used for both arc and static field delivery, but only simulation results have been reported so far.

The purpose of this study was to experimentally quantify the geometric accuracy of a novel real-time 3D target localization method (Cho *et al* 2010) using sequential kV imaging combined with respiratory monitoring for clinically realistic arc and static field treatment delivery and target motion conditions. Compared to previous localization methods that rely partly on MV images, the current method allows arbitrary intensity modulation. Compared to localization methods that rely only on x-ray images, the current method results in reduced imaging dose due to the addition of external respiratory monitoring.

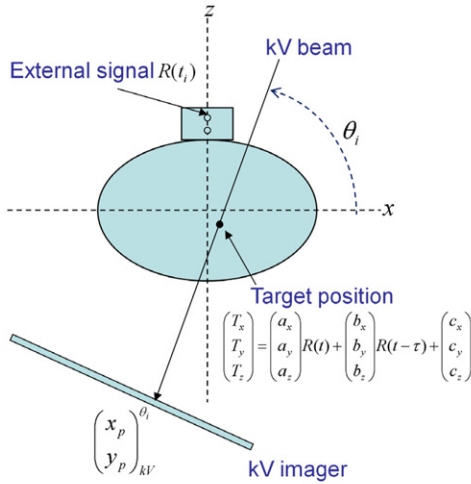
Method and materials

Target localization algorithm

The theory and simulation results of the localization method have previously been described (Cho *et al* 2010). They are reviewed briefly here to support the experimental investigation in the current work. The 3D target position $\mathbf{T}(x, y, z; t)$ is estimated from the respiratory signal $R(t)$ through the correlation between $R(t_i)$ and the projected marker positions $\mathbf{p}(x_p, y_p; t_i)$ on kV images by a state-augmented linear model (Ruan *et al* 2008): $\mathbf{T}(x, y, z; t) = \mathbf{a}R(t) + \mathbf{b}R(t - \tau) + \mathbf{c}$. The model parameters, \mathbf{a} , \mathbf{b} , \mathbf{c} , are determined by solving a least-squares estimation of the 2D error $\sum \|\mathbf{p}(x_p, y_p; t_i) - \mathbf{P}(\theta_i) \cdot (\mathbf{a}R(t_i) + \mathbf{b}R(t_i - \tau) + \mathbf{c})\|^2$. Here, $\mathbf{P}(\theta_i)$ is a projection operator onto the i th kV image of the gantry angle θ_i and the lag time τ was set 0.5 s. The model is initiated by acquiring kV projections in an arc of 120° prior to MV beam delivery. The steps, equations and term definitions are shown in figure 1.

Experimental system and method

The localization method is integrated into a prototype DMLC tracking system consisting of an OBI x-ray imager (operating at 1 Hz in this study), RPM respiratory signal (30 Hz) and Trilogy linac equipped with a Millennium 120-leaf MLC (Varian Medical Systems, Palo Alto, CA). The process is shown in figure 2. In step 1 of figure 2 the kV images are acquired, then saved (step 2). An in-house developed marker extraction program opens the images and segments the marker positions (step 3). The 2D marker positions and the projection angle, along with the respiratory signal (step 4) are sent to the 3D position estimation model (step 5) described above. It also includes a motion prediction module (Srivastava *et al* 2007) applied to the respiratory signal to compensate for the 160 ms system latency (the time between the occurrence of motion and the MLC response). The prediction algorithm uses a modified linear adaptive filter and reduces the error induced by the latency by 30% on average. The calculated 3D target location is sent to the DMLC tracking program (step 6) where the DMLC positioning algorithm (Sawant *et al* 2008) integrates the 3D target location with the planned leaf sequence. The updated leaf sequence is then sent to the DMLC controller (step 7) and the MLC to align the beam with the target. Note that the 160 ms system latency is the same as that measured for the RPM input (Keall *et al* 2006), rather than the 1090 ms latency of the 1 Hz OBI input alone (Poulsen *et al* 2010a, Poulsen *et al* 2010b). The time difference between the signals is accounted for in the model by synchronizing them together. The effect is a 930 ms delay in the *updating* of the model, but not in the *use* of the model for real-time 3D target localization.



(1) Projected position measurement

$$\begin{pmatrix} x_p \\ y_p \end{pmatrix}_{kV}^{\theta_i} = \frac{1}{f(\theta_i)} \begin{pmatrix} \cos \theta_i \cdot T_x + \sin \theta_i \cdot T_z \\ T_y \end{pmatrix}$$

$$f(\theta_i) = \frac{[SAD - (-\sin \theta_i \cdot T_x + \cos \theta_i \cdot T_z)]}{SAD} \cong 1$$

(2) Correlation model

$$T_x(t_i) = a_x R(t_i) + b_x R(t_i - \tau) + c_x$$

(3) Parameter estimate (LSE)

$$\arg \min \sum_i^N \left\| x_p(t_i) - \frac{1}{f(\theta_i)} [\cos \theta_i \cdot T_x + \sin \theta_i \cdot T_z] \right\|^2$$

$$\arg \min \sum_i^N \left\| y_p(t_i) - \frac{1}{f(\theta_i)} T_y(t_i) \right\|^2$$

(4) Target position estimation

$$\hat{T}_x(t) = \hat{a}_x R(t) + \hat{b}_x R(t - \tau) + \hat{c}_x$$

Figure 1. Schematic diagram showing the procedure of real-time target localization. Each direction of internal target motion $\mathbf{T}(x, y, z; t)$ was estimated from the external respiratory signal $R(t)$ through the correlation between $R(t_i)$ and the projected marker positions $\mathbf{p}(x_p, y_p; t_i)$ on kV images by a state-augmented linear model: $\mathbf{T}(x, y, z; t) = \mathbf{a}R(t) + \mathbf{b}(t - \tau) + \mathbf{c}$. The model parameters were determined by solving a least-squares estimation (LSE) of the error $\sum \|\mathbf{p}(x_p, y_p; t_i) - \mathbf{P}(\theta_i) \cdot (\mathbf{a}R(t_i) + \mathbf{b}R(t_i - \tau) + \mathbf{c})\|^2$ with projection operator $\mathbf{P}(\theta_i)$ (Cho *et al* 2010). Prior to treatment, rotational kV imaging of 120° was sequentially acquired to initialize the estimation model and start the estimation. The model parameters were updated every time a new kV image was acquired with the kV projection data covering 120° angular span. SAD = source-axis distance (100 cm in this study).

Each experiment started with training of the prediction algorithm to compensate the 160 ms system delay. This training involved acquiring the external respiratory signal (RPM in our case) for 40 s. Subsequently, the initial correlation model between the marker position on kV images and synchronized RPM signal was built by rotating the gantry through 120° with the kV imager on.

Ten tumour trajectories and associated external respiratory signals with a motion range larger than 10 mm were selected from 160 tumour trajectories (Suh *et al* 2008). The dataset was acquired from 46 thoracic and abdominal tumour patients treated by a CyberKnife Synchrony system. The mean (range) of the peak-to-peak motion of the selected trajectories was 6.4 (1.2–20.8) mm, 13.0 (1.0–20.4) mm, and 5.7 (1.8–13.7) mm in the left-right (LR), superior-inferior (SI) and anterior-posterior (AP) directions, respectively. The mean (range) of their average breathing cycles was 3.8 (2.7–4.9) s. Note, this dataset was the same as that used for a previous experimental tracking study combining kV, MV and the respiratory signal (Cho *et al* 2011).

A 358° -arc plan and a static five-field plan were delivered to a 4D phantom from Washington University (Malinowski *et al* 2007). The phantom consists of a 3D moving phantom which was programmed to reproduce each of the ten tumour trajectories, and an independent 1D moving phantom that was simultaneously programmed to reproduce the patient-measured anterior-posterior external abdominal breathing motion. The arc plan started in a counter-clockwise manner with the gantry starting at 1° and ending at 359° . The five beam angles of the static plan were 0° , 72° , 144° , 216° , and 288° (Varian scale). The timeline of the gantry angle position for the arc and static fields is shown in figure 3. The beam delivery

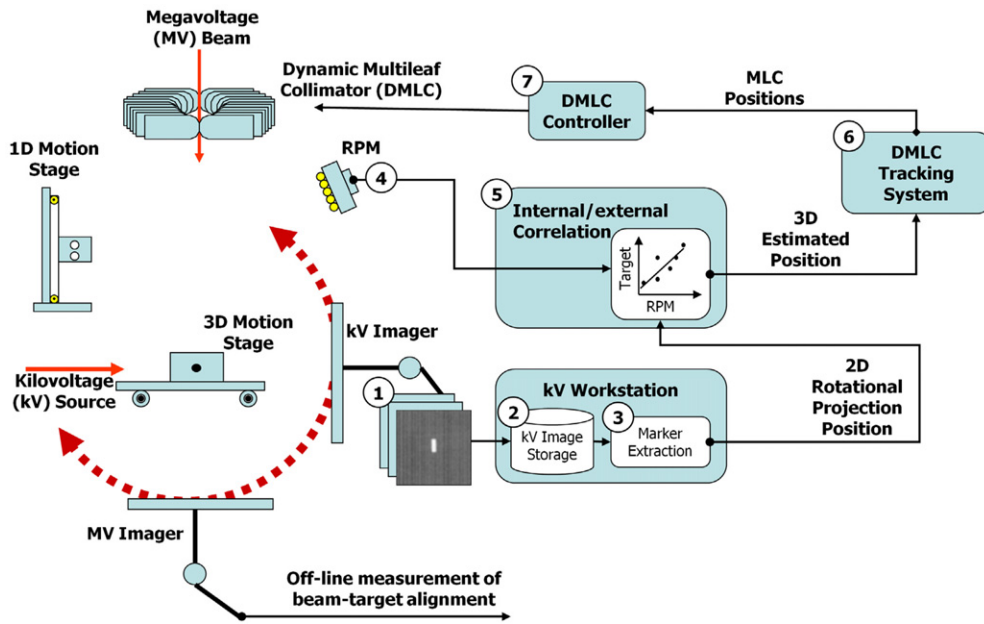


Figure 2. Flowchart for the real-time target localization and beam adaptation measurements.

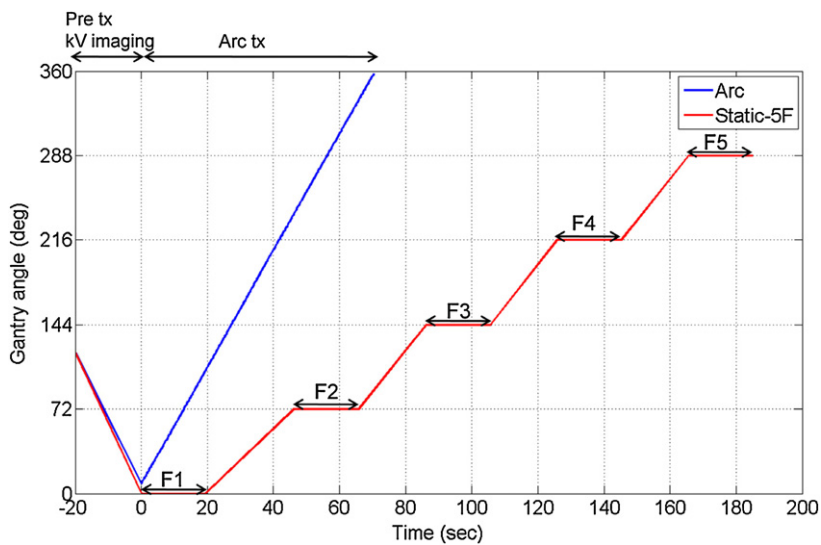


Figure 3. Gantry angle versus time for the arc and static five-field beam delivery experiments. Prior to treatment onset, from -20 to 0 s in the plot, rotational kV images over 120° are acquired at 1 Hz along with the respiratory signal and are used to initialize the localization method. For arc delivery, the MV beam was delivered in ~ 72 s from gantry angle 1° to 359° . For the five-field treatment the MV beam was delivered for 20 s at each of five even-spaced gantry angles.

time was set to 60 s for the arc plan and 20 s for each of the five fields in the static plan. The MLC-shaped circular field was used for both plans. Fluoroscopic kV images were acquired at 1 Hz perpendicular to the treatment beam axis during a 120° pre-treatment gantry rotation,

during treatment delivery and, for the static five-field plan, during inter-field gantry rotations. The 120° rotational kV imaging prior to treatment was used to initialize the correlation model for both the arc and static plans, as shown in the -20 to 0 s part of figure 3. It was based on the finding of the previous simulation study (Cho *et al* 2010) that at least 120° rotational kV imaging is necessary for minimal parallax error. For the same reason, the data window for the model computation was fixed so that the projection data covered an angular span of 120° instead of fixing the time interval. Therefore, the estimation error would likely be higher for the static plan than the arc plan because the temporal change of the correlation would not be adapted to as promptly.

The accuracy of the localization method was investigated by quantifying the beam-target positional error, during arc and static beam delivery, for each of the ten traces. The MV imager was used as an independent measurement tool where the beam aperture and the target position, represented by a fiducial marker, were visible in each image. The MV images were acquired in cine mode at 3.4 Hz, which was determined empirically to obtain appropriate kV image quality while the MV beam was on. This measurement method has been described previously (Cho *et al* 2009). The beam-target alignment error with real-time localization was quantified by measuring the geometric distance between the centre of the circular beam aperture and fiducial marker on each MV image as a function of time. The error without real-time localization was quantified as the distance between the fiducial marker and the position of the beam aperture centre as it would have been if no MLC refitting were applied.

Results

Typical examples of the target and aperture position as a function of time are shown in figures 4 and 5 for the arc and static beam delivery, respectively. They are the same trajectory examples chosen in the previous tracking study combining kV, MV and the respiratory signal (Cho *et al* 2011), to represent characteristics of fast breathing, irregular amplitude, and baseline drift in respiratory motion. In figure 4, the apparent variation in the horizontal motion with time is due to the changing motion projection during the treatment delivery with the rotating gantry. The 2D root-mean-squared (rms) beam-target errors for all ten tumour motion traces during both the arc and static field delivery with and without real-time localization are summarized in figure 6. The overall error was substantially reduced with real-time localization: the beam-target 2D error of 4.9 ± 1.0 mm (1σ) without real-time localization was reduced to 1.0 ± 0.2 mm (1σ) with localization for both the arc and static beam delivery, approximately an 80% reduction in both cases. In addition to an overall reduction in beam-target error, the patient-to-patient variation without real-time localization of 4.2 mm (range 3.1–7.3 mm) was reduced to 1.0 mm (range 0.7–1.4 mm). This reduction in the patient-to-patient variability indicates that a more stable estimate can be made of the margin needed to account for targeting errors.

The residual localization error is mainly attributed to the accuracy of the correlation model, the system latency (partially corrected using the prediction algorithm), gantry sag and the alignment of the kV imager with respect to the beam isocentre. To learn more about the contributions from each of the components, their performances were separately investigated. To examine the accuracy of the correlation model, each time a kV or MV image was acquired the measured position projected on the image was compared with the position estimated by the correlation model using the synchronized RPM signal. The estimation accuracy of the correlation model for the all experiments was ~ 0.5 mm in each direction. It demonstrates that even with a single kV imager the overall accuracy was similar to a previous study using the respiratory signal and both kV and MV imagers for stereoscopic imaging (Cho *et al* 2011). This value is already close to the limit of the machine accuracy, i.e. gantry sag and the alignment

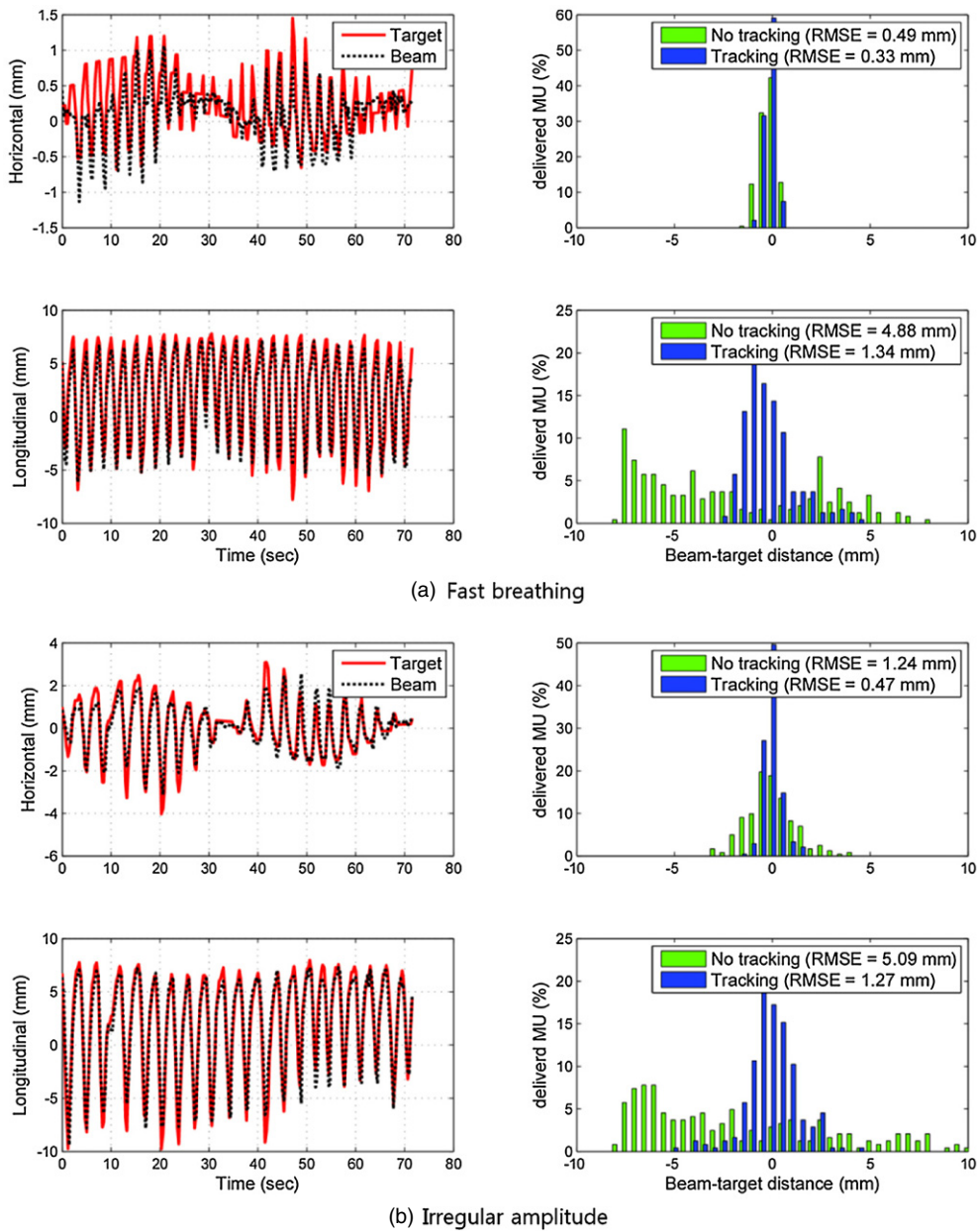


Figure 4. The MV imager measured target position, aperture position and tracking error of three typical tumour motion traces during arc delivery featuring (a) fast breathing, (b) irregular amplitude and (c) baseline drifts during the beam delivery. The left column shows the trajectory of the marker and the following MLC aperture in each direction on MV images: the horizontal position corresponds to motion perpendicular to the MV imager in the axial patient plane; the longitudinal position corresponds to motion in the SI direction. The right column shows histograms of tracking error without (no tracking) and with (tracking) real-time localization.

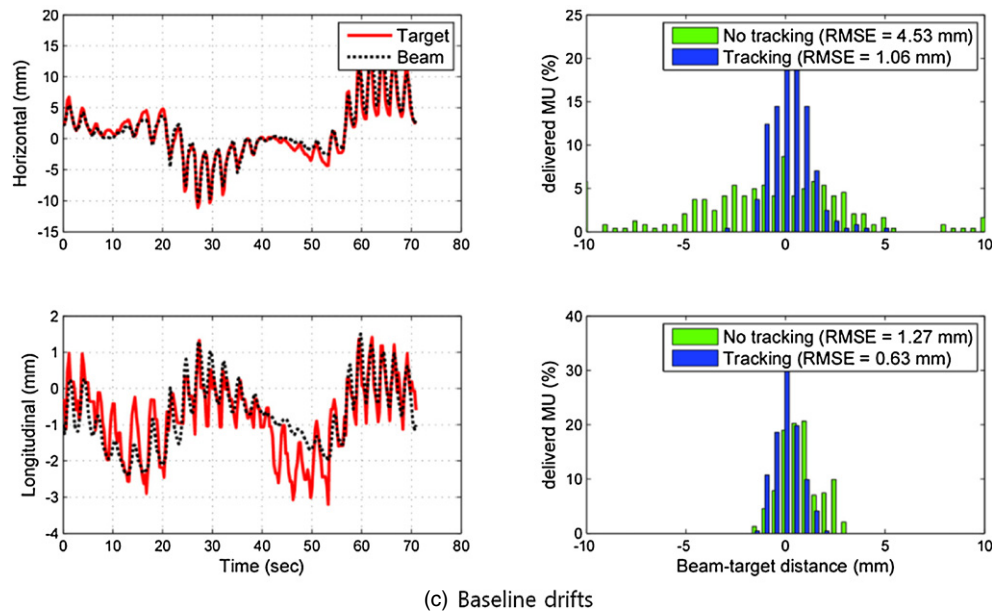


Figure 4. (Continued.)

of the kV imager with respect to the beam isocentre. It should be noted that another important factor determining the accuracy of the correlation model would be the degree of strength in the individual correlation between the internal target movement and the external respiratory signal.

To assess the performance of the prediction algorithm, the predicted external respiratory signals were recorded with the measured values. The prediction error was computed from the difference between the predicted value and the measured value shifted 160 ms. Overall, the error due to the system latency was reduced by 30% by applying the prediction algorithm, even though the error due to the system latency was small, <1 mm, because of the relatively short latency.

Discussion

Many devices and methods are available for real-time target localization. However, the clinical integration of these methods to control the treatment beam and align the radiation beam and treatment target is to date limited to the Cyberknife and Vero systems. In this study, a new real-time 3D localization method (Cho *et al* 2010) was integrated into a prototype DMLC-based tumour tracking system to obtain the first experimental results of the real-time localization algorithm. The localization method utilizes data from a kV imager and an optical respiratory monitoring signal, both widely available on many IGRT platforms. The localization method is fully compatible with intensity modulation (IMRT and VMAT) since the use of MV portal images is avoided. It allows a large reduction in the imaging frequency and, thus the imaging dose as compared to methods that solely relying on x-ray imaging. Experimental validation of the localization method was performed using clinically realistic arc and static field treatment delivery conditions to a phantom containing an implanted marker. The phantom was programmed to reproduce measured tumour motion data. An independent

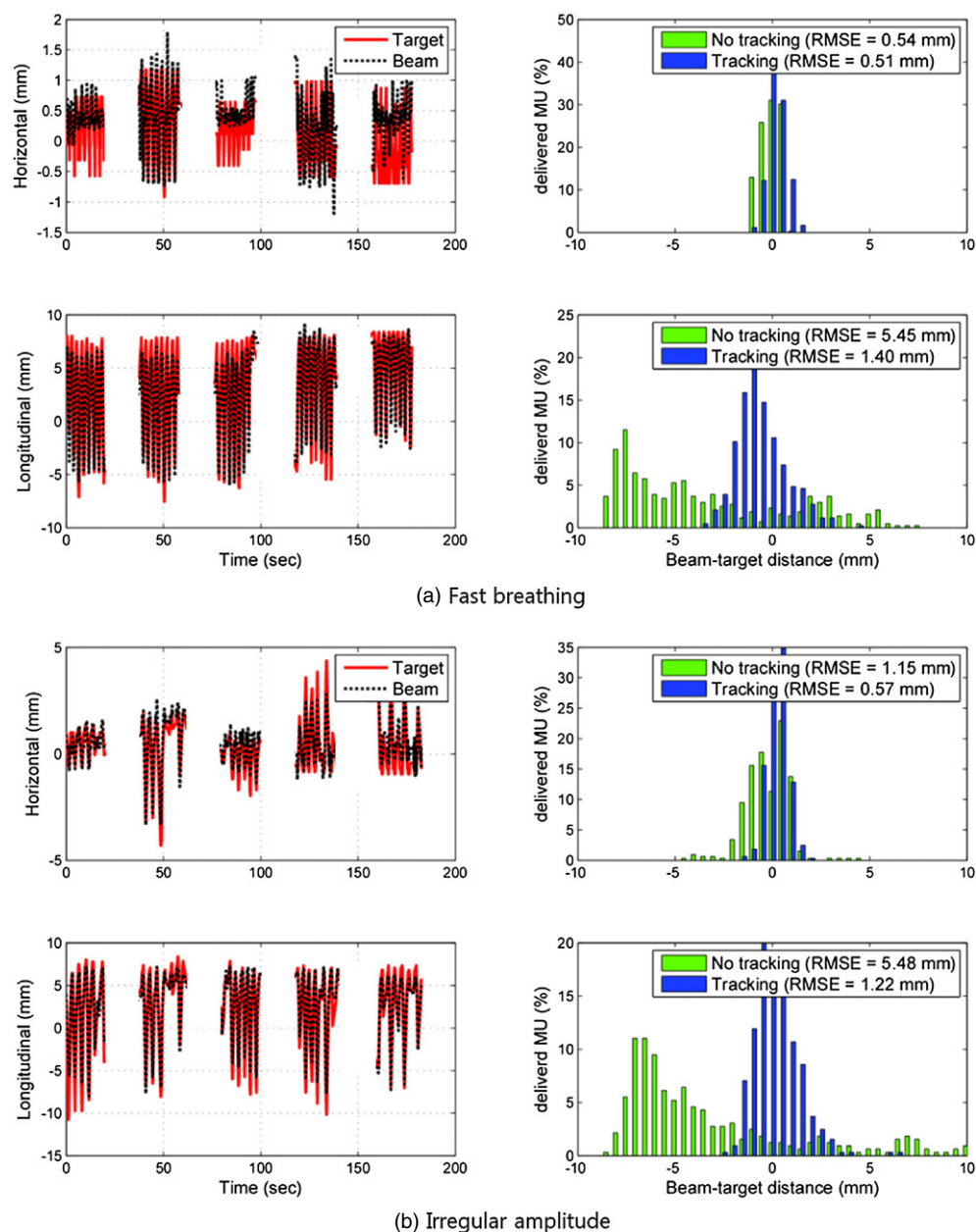


Figure 5. The MV imager measured target position, aperture position and tracking error of three typical tumour motion traces during five-field delivery featuring: (a) fast breathing, (b) irregular amplitude and (c) baseline drifts during the beam delivery. The left column shows the trajectory of the marker and the following MLC aperture in each direction on MV images, where the longitudinal position corresponds to motion in the SI direction. The right column shows histograms of tracking error without (no tracking) and with (tracking) real-time localization.

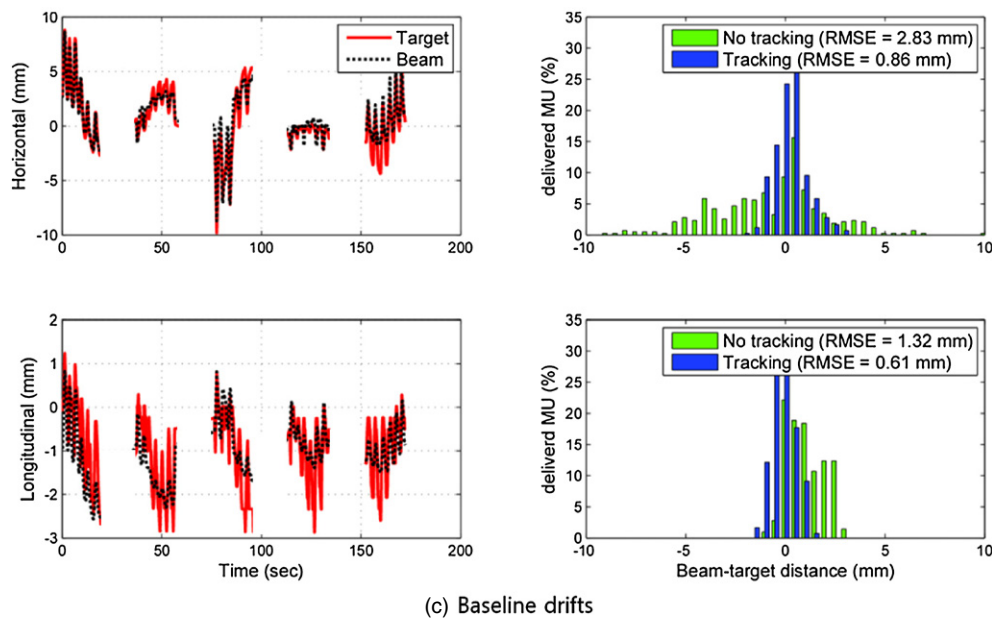


Figure 5. (Continued.)

axis was programmed to reproduce synchronously measured respiratory motion. Average beam-target geometric errors of 1 mm were observed.

This method, in its current form, requires marker implantation which is similar to other marker-based methods including those employed by BrainLab, Calypso, Cyberknife, and Navotek. Potentially, marker-free kV imaging could be used to image the tumour location directly (Lin *et al* 2009, Berbeco *et al* 2005). However, any uncertainties in the tumour segmentation will be translated to beam-target alignment errors. In applying these results to a clinical scenario, the biggest difference is the accuracy of marker segmentation. For the current application, a marker was embedded in a uniform phantom, making the marker segmentation simpler and more reliable than clinical segmentation in which there is a heterogeneous background.

An important clinical issue with using kV for guidance is the additional imaging dose. From AAPM Task Group 75 (Murphy *et al* 2007), the dose per image based on the Synchrony system is 0.05–0.25 mGy. In addition to ensuring the exposure settings are optimal, large dose reductions can be made by limiting the kV field to the target and reducing the image frequency. In this experimental study, the kV imager was operating at 1 Hz. From figure 3, this would result in 100 images for the arc treatment and 200 images for the static field treatment. In the simulation paper of this localization method, when the imaging frequency was reduced from once per second to once every 10 s, a 25% increase in geometric error was observed, at the reduction of an order of magnitude of imaging dose (Cho *et al* 2010). The optimal kV imaging frequency for clinical implementation which trades off accuracy with dose remains to be determined.

Should clinical marker segmentation prove similar in accuracy to these experiments, we can anticipate that the total system accuracy could be improved to have sub-mm error on a system specifically designed for real-time tracking of respiratory motion. For example, reducing the system latency (160 ms for this system), better kV/MV alignment, lower gantry

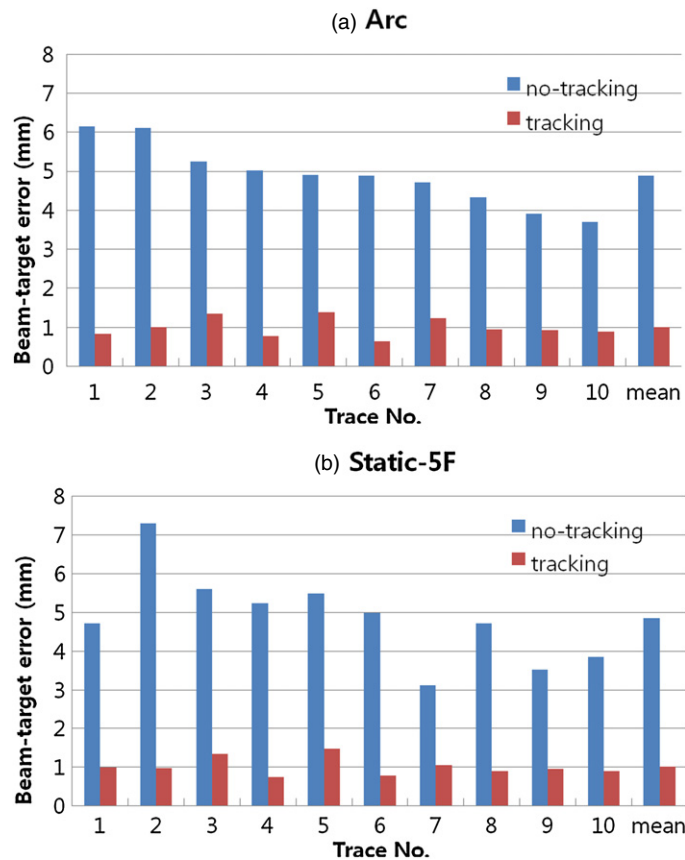


Figure 6. Summary of the 2D rms tracking errors for the ten lung tumour motion traces measured using cine MV images during the (a) arc and (b) static five-field beam delivery without (no tracking) and with (tracking) real-time localization. DMLC tracking integrated with the proposed localization method showed ~ 1 mm of mean rms error irrelevant of the beam delivery modes or the range of motion.

sag (or gantry sag compensation by MLC adjustment) and improved prediction algorithms would all help to reduce the beam-target error. Given that the inter-observer variations in target delineation (4–10 mm) (Steenbakkers *et al* 2006) are of the order of the error of the treatment accuracy without real-time localization, further reductions in error at the sub-mm level may have limited clinical benefit at this time.

Conclusion

The first experimental study of a novel real-time 3D target localization method using sequential kV imaging combined with optical respiratory monitoring on a Varian linear accelerator has been performed. Average geometric errors of 1 mm were observed for clinically realistic arc and static field treatment delivery conditions for ten patient-derived tumour and respiratory motion traces. These errors could be further reduced with improved kV/MV alignment and lower system latency. The localization method can also be applied to other IGRT systems, including those from Accuray, BrainLab and Elekta.

Acknowledgments

The authors gratefully acknowledge the support of US NIH/NCI R01-93626 and an NHMRC Australia Fellowship. BC was supported by Basic Science Research Program through the National Research Foundation of Korea (NRF) funded by the Ministry of Education, Science and Technology (2011-26369). Thank you to Julie Baz, University of Sydney, for reviewing the manuscript. The authors thank the following contributors from Varian Medical Systems: Herbert Cattell, for substantial development of the DMLC adaptation program, Hassan Mostafavi and Alexander Sloutsky, for the marker extraction software used for offline image analysis and Sergey Povzner for the RPM communication interface development.

References

- Berbeco R I, Jiang S B, Sharp G C, Chen G T, Mostafavi H and Shirato H 2004 Integrated radiotherapy imaging system (IRIS): design considerations of tumour tracking with linac gantry-mounted diagnostic x-ray systems with flat-panel detectors *Phys. Med. Biol.* **49** 243–55
- Berbeco R I, Mostafavi H, Sharp G C and Jiang S B 2005 Towards fluoroscopic respiratory gating for lung tumours without radiopaque markers *Phys. Med. Biol.* **50** 4481
- Cho B, Poulsen P R and Keall P J 2010 Real-time tumor tracking using sequential kV imaging combined with respiratory monitoring: a general framework applicable to commonly used IGRT systems *Phys. Med. Biol.* **55** 3299–316
- Cho B, Poulsen P R, Sawant A, Ruan D and Keall P J 2011 Real-time target position estimation using stereoscopic kilovoltage/megavoltage imaging and external respiratory monitoring for dynamic multileaf collimator tracking *Int. J. Radiat. Oncol. Biol. Phys.* **79** 269–78
- Cho B, Poulsen P R, Sloutsky A, Sawant A and Keall P J 2009 First demonstration of combined kV/MV image-guided real-time dynamic multileaf-collimator target tracking *Int. J. Radiat. Oncol. Biol. Phys.* **74** 859–67
- Cho B, Suh Y, Dieterich S and Keall P J 2008 A monoscopic method for real-time tumour tracking using combined occasional x-ray imaging and continuous respiratory monitoring *Phys. Med. Biol.* **53** 2837
- Hoogeman M, Prévost J-B, Nuytens J, Pöll J, Levendag P and Heijmen B 2009 Clinical accuracy of the respiratory tumor tracking system of the cyberKnife: assessment by analysis of log files *Int. J. Radiat. Oncol. Biol. Phys.* **74** 297–303
- Isaksson M, Jalden J and Murphy M J 2005 On using an adaptive neural network to predict lung tumor motion during respiration for radiotherapy applications *Med. Phys.* **32** 3801–9
- Kamino Y, Takayama K, Kokubo M, Narita Y, Hirai E, Kawawada N, Mizowaki T, Nagata Y, Nishidai T and Hiraoka M 2006 Development of a four-dimensional image-guided radiotherapy system with a gimbaled x-ray head *Int. J. Radiat. Oncol. Biol. Phys.* **66** 271–8
- Kanoulas E, Aslam J A, Sharp G C, Berbeco R I, Nishioka S, Shirato H and Jiang S B 2007 Derivation of the tumor position from external respiratory surrogates with periodical updating of the internal/external correlation *Phys. Med. Biol.* **52** 5443–56
- Keall P J, Cattell H, Pokhrel D, Dieterich S, Wong K H, Murphy M J, Vedam S S, Wijesooriya K and Mohan R 2006 Geometric accuracy of a real-time target tracking system with dynamic multileaf collimator tracking system *Int. J. Radiat. Oncol. Biol. Phys.* **65** 1579–84
- Lam K, Hadley S and Balter J 2009 IBreathe: monitoring respiration with the accelerometer in an iPod Touch *Med. Phys.* **36** 2489 (abstract)
- Lin T, Li R, Tang X, Dy J G and Jiang S B 2009 Markerless gating for lung cancer radiotherapy based on machine learning techniques *Phys. Med. Biol.* **54** 1555
- Malinowski K, Noel C, Lu W, Lechleiter K, Hubenschmidt J, Low D and Parikh P 2007 Development of the 4D Phantom for patient-specific, end-to-end radiation therapy QA *Phys Med Imaging* **6510** 65100E-9
- Murphy M J 2004 Tracking moving organs in real time *Semin. Radiat. Oncol.* **14** 91–100
- Murphy M J *et al* 2007 The management of imaging dose during image-guided radiotherapy: report of the AAPM task group 75 *Med. Phys.* **34** 4041–63
- Poulsen P R, Cho B, Ruan D, Sawant A and Keall P J 2010a Dynamic multileaf collimator tracking of respiratory target motion based on a single kilovoltage imager during arc radiotherapy *Int. J. Radiat. Oncol. Biol. Phys.* **77** 600–7
- Poulsen P R, Cho B, Sawant A and Keall P J 2010b Implementation of a new method for dynamic multileaf collimator tracking of prostate motion in arc radiotherapy using a single kV imager *Int. J. Radiat. Oncol. Biol. Phys.* **76** 914–23

- Poulsen P R, Cho B, Sawant A, Ruan D and Keall P J 2010c Dynamic MLC tracking of moving targets with a single kV imager for 3D conformal and IMRT treatments *Acta Oncol.* **49** 1092–100
- Ruan D, Fessler J A, Balter J M, Berbeco R I, Nishioka S and Shirato H 2008 Inference of hysteretic respiratory tumor motion from external surrogates: a state augmentation approach *Phys. Med. Biol.* **53** 2923
- Sawant A, Venkat R, Srivastava V, Carlson D, Povzner S, Cattell H and Keall P 2008 Management of three-dimensional intrafraction motion through real-time DMLC tracking *Med. Phys.* **35** 2050–61
- Schweikard A, Glosner G, Bodduluri M, Murphy M J and Adler J R 2000 Robotic motion compensation for respiratory movement during radiosurgery *Comput. Aided Surg.* **5** 263–77
- Shirato H *et al* 2000a Four-dimensional treatment planning and fluoroscopic real-time tumor tracking radiotherapy for moving tumor *Int. J. Radiat. Oncol. Biol. Phys.* **48** 435–42
- Shirato H *et al* 2000b Physical aspects of a real-time tumor-tracking system for gated radiotherapy *Int. J. Radiat. Oncol. Biol. Phys.* **48** 1187–95
- Siwiak D, Berger J and Yang Y 2009 Catch your breath: musical biofeedback for breathing regulation *Proc. 9th Int. Conf. New Interfaces for Musical Expression (Pittsburgh, PA)* pp 153–4
- Srivastava V, Keall P, Sawant A and Suh Y 2007 Accurate prediction of intra-fraction motion using a modified linear adaptive filter *Med. Phys.* **34** 2546
- Steenbakkens R J *et al* 2006 Reduction of observer variation using matched CT-PET for lung cancer delineation: a three-dimensional analysis *Int. J. Radiat. Oncol. Biol. Phys.* **64** 435–48
- Suh Y, Dieterich S, Cho B and Keall P J 2008 An analysis of thoracic and abdominal tumour motion for stereotactic body radiotherapy patients *Phys. Med. Biol.* **53** 3623–40